Traffic Sign Occlusion Detection Using Mobile Laser Scanning Point Clouds

Pengdi Huang, Ming Cheng, *Member, IEEE*, Yiping Chen, Huan Luo, Cheng Wang, *Senior Member, IEEE*, and Jonathan Li, *Senior Member, IEEE*

***Abstract*— For survey and maintenance of traffic signs, this paper presents a novel traffic sign occlusion detection method using 3-D point clouds and trajectory data acquired by a mobile laser scanning system. To produce a maintenance guide, our method aims to obtain the degree of occlusion by analyzing the spatial relationship between traffic signs, surroundings, and drivers on the road. First, a detection method considering both reflectance and geometric features is developed to capture traffic signs. Next, to simulate the driver's view, a trajectory-based method is proposed to determine driver's observation location and the corresponding observed traffic sign. Finally, to determine whether a traffic sign is in occlusion, a hidden point removal algorithm is adopted and carried out. Furthermore, we develop two indices to evaluate the degree of occlusion. The proposed method is tested using two point cloud data sets collected by an RIEGL VMX-450 system along a 23.68-km-long urban road. The obtained results illustrate the feasibility of the proposed occlusion detection method.**

***Index Terms*— Occlusion detection, mobile laser scanning (MLS), hidden point removal (HPR) operator, 3D point clouds, traffic sign.**

I. Introduction

TRAFFIC signs are mounted on both sides of the road, and provide compact information about road conditions and traffic regulations. However, visual occlusion may result in delayed or even no observation of traffic signs for drivers. To reduce the risk of traffic accidents, periodically inspecting occlusion of traffic signs is one of the maintenance tasks. Thus, this paper is to present a traffic sign occlusion system which provides a maintenance guide for traffic facility maintainer and planner. "Occlusion" is defined as a status that an obstacle is in the line-of-sight between a driver and a traffic sign at certain moment during driving.

Manuscript received March 31, 2016; revised July 23, 2016 and November 15, 2016; accepted December 9, 2016. Date of current version August 28, 2017. This work was supported in part by the National Natural Science Foundation of China under Grant 41471379 and in part by the Fujian Collaborative Innovation Center for Big Data Applications in Governments. The Associate Editor for this paper was D. Fernandez-Llorca. *(Corresponding authors: Ming Cheng and Jonathan Li.)*

P. Huang, M. Cheng, Y. Chen, H. Luo, and C. Wang are with Fujian Key Laboratory of Sensing and Computing for Smart Cities, School of Information Science and Engineering, Xiamen University, Xiamen 361005, China (e-mail: alualu628628@163.com; chm99@xmu.edu.cn; ypchenhk@gmail.com; scholar.luo@gmail.com; cwang@xmu.edu.cn).

J. Li is with Fujian Key Laboratory of Sensing and Computing for Smart Cities, School of Information Science and Engineering, Xiamen University, Xiamen 361005, China, and also with the Department of Geography and Environmental Management, University of Waterloo, Waterloo, ON N2L 3G1, Canada (e-mail: junli@uwaterloo.ca).

Color versions of one or more of the figures in this paper are available online at http://ieeexplore.ieee.org.

Digital Object Identifier 10.1109/TITS.2016.2639582

The main causes of traffic sign occlusion are the interferences from other objects alongside the road (e.g., plants, billboards, pipelines). To ensure the visual saliency of traffic signs is a mandatory requirement of road facility maintenance, and some regulations [1], [2] demand that a necessary distance should be kept between traffic signs and other objects. However, invasion from slow-growing plants is difficult to detect and control timely. In addition, the traditional manual occlusion detection methods are inefficient and difficult to quantify the exact extent of occlusion from the perspective of the driver.

The application of computer vision has received more and more attention in recent years. Previous traffic sign investigations mainly focused on image or video data. For driver assistance systems, a traffic sign recognition method, including traffic sign detection and classification, was usually adopted based on various features and classifiers (summarized in [3]). Some researches on the visibility of traffic sign focused on how obvious a traffic sign was in relation to its surroundings (conspicuity) [4]. The evaluation was intended to prompt easily-missed signs only and to avoid driver distraction. Moreover, in other visibility work, the display quality of traffic signs has come under study. Methods of inspecting text (e.g., symbols [5], words [6]) and reflection values [7] on road signs or panels have also been developed to reduce the risks of manual inspection. However, to the best of our knowledge, there is little report about targeted work of traffic sign occlusion inspection. In fact, occlusions tend to be considered as an unstable condition or negative factor for sign detection in image processing.

Unlike optical imaging in which occlusion may cause data loss, 3D laser scanning is specialized in preserving the integrity of objects by means of multi-station scanning, registering, and stitching. Mobile laser scanning (MLS) provides a simple and efficient approach to obtain a full-view perspective of road scene. To obtain the complete data of an obstructed object, MLS benefits from two aspects: 1) The laser pulse can pass through small gaps in a vegetation canopy or leaves, and return the reflection of an object behind the canopy [8]; 2) The "full circle" scanning pattern of MLS provides 360° scanning for seamless and complete point clouds data in a road scene. Traffic sign detection in point clouds acquired by a RIEGL VMX-450 system has been proved to be unsusceptible to occlusion [9]. Fig. 1 illustrates various occlusions occurring to several different traffic signs, which our method intends to detect and provide alerts for. The traffic signs (in red box) are partially lost in the images, but are kept intact (in blue circle)

1524-9050 © 2017 IEEE. Personal use is permitted, but republication/redistribution requires IEEE permission.
See http://www.ieee.org/publications_standards/publications/rights/index.html for more information.

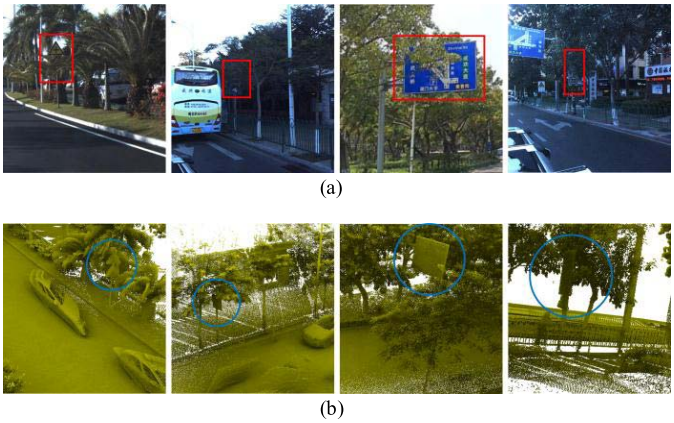

Fig. 1. Traffic signs with various occlusions: (a) partial loss of traffic signs caused by occlusion in images, (b) data integrity maintained in MLS point clouds.

in the point clouds, even though occlusion appeared in the same viewpoints (driver eyes).

The contribution of this paper is the presentation of a framework for analyzing traffic sign occlusions from MLS point cloud data. The main novelties of our work are as: First and foremost, we proposed an approach to detect traffic sign occlusion from a series of carefully selected viewpoints, and defined two indexes for further analysis of the impact of occlusion. The second novelty of the work is that a driver perspective-based method is developed to simulate the true sight of the driver in point cloud scene. Thirdly, a point-based detecting method with growth repair was designed to detect traffic signs from hostile surroundings.

The rest of the paper is organized as follows. A review of the previous work on traffic sign inspection in point clouds is given in Section II. The methodology of our framework is described and presented in Sections III, in which traffic sign detection, observation planning, and occlusion detection and analysis are detailed in Subsection *A*, *B*, and *C*, respectively. Experimental results and conclusions are presented in Sections IV and V, respectively.

II. Related Work

Traffic sign inspection in point clouds makes rapid progress in recent years. Traffic sign parameters (e.g., type, tilted angle, and position) extraction is becoming a hot topic for study. However, there is few research work on the analysis of traffic sign occlusion. The analysis of occlusion measures the spatial relationship among traffic signs, drivers, and the environment, in which traffic signs must be detected first. In this section, we will give a brief review of literature on detection of traffic signs.

Traffic signs, regarded as one category of urban road object, are detected by generic classification method of scene object in literature. A system was designed in [10] to recognize small objects from urban point clouds, in which each individual object was labeled after locating and segmenting from the raw data. Then, various features (e.g., shape and context) of the labeled objects were calculated, and a classifier was used to perform object recognition (including traffic signs). In order to detect road facilities, Yu *et al.* [11] preferred matching rather than classifying. Yang and Dong [12] used dimensional features and min cuts to form topological units, and the topological units were merged to construct various objects in point clouds. As an improvement of [12], a more robust method was presented in [13] based on multi-scale supervoxels to detect urban objects, including traffic signs. The implicit shape model and Hough forest were applied in [14] to locate the center of objects (e.g., traffic signs, cars, and light poles).

In some studies, traffic signs were considered as the pole-like objects. In this case, pole detecting is promoted to a main detecting clue. A scan line based method was developed in [15] to cluster and classify poles from MLS point clouds. A quartiles height percentile method was designed in [16] to detect vertical pole-like objects, and a fitted geometric comparison method was proposed to recognize the planar shapes of signs. In [17], pole-like objects were first segmented and grouped, and then noise was removed by endpoint preserving Laplacian smoothing method. After that, an object evaluated function considering attachment types, shapes, and context features was designed to recognize pole-like objects. Traffic signs were extracted in [9] by finding the linear structure of pole-like objects, and then objects other than traffic signs (e.g., light poles or trees) were removed through intensity filtering. Several geometric and positional parameters (e.g., height, tilted angle, degree of flatness) of traffic signs were acquired at last.

Some studies focused on extracting the traffic sign panel whereas discarding the connecting pole. Gonzalez-Jorge *et al.* [18] used a terrestrial laser scanner to inspect folded and tilted signs. An intensity based segmentation algorithm was used to extract sign points, and the deviation between the fitted and ideal sign planes was calculated to evaluate the flatness of the sign's front face. Furthermore, tilt evaluation was used to check whether the fitted plane's normal vector was parallel to the ground. Chen *et al.* [19] segmented signs from point clouds by intensity information, and a grid-based cluster algorithm was designed to determine the size of the panel on a fitting plane. To strictly detect traffic signs in MLS point clouds, Ai and Tsai [20] conducted a multi-filter process, in which the parameters used for filtering included retro-intensity, elevation, lateral offset, and hit counting.

For the following two reasons, the traffic sign pole should be omitted from the results of the traffic sign extraction in our occlusion analysis method: 1) If the pole is included in the traffic sign extraction results, an occlusion will be detected between the pole and the board in front since the former is occluded by the latter, which is a false alarm. 2) Low vegetation around the traffic sign pole cannot affect the driver's sight, but may generate a false alarm in the analysis result. Hence, detection methods that contain pole points in the results are not suitable for our research. We develop a board detection method that accurately labels the points belonging to the traffic sign board. In the rest of this paper, the term "traffic sign" denotes only the traffic sign board or panel, not the entire structure with a pole.

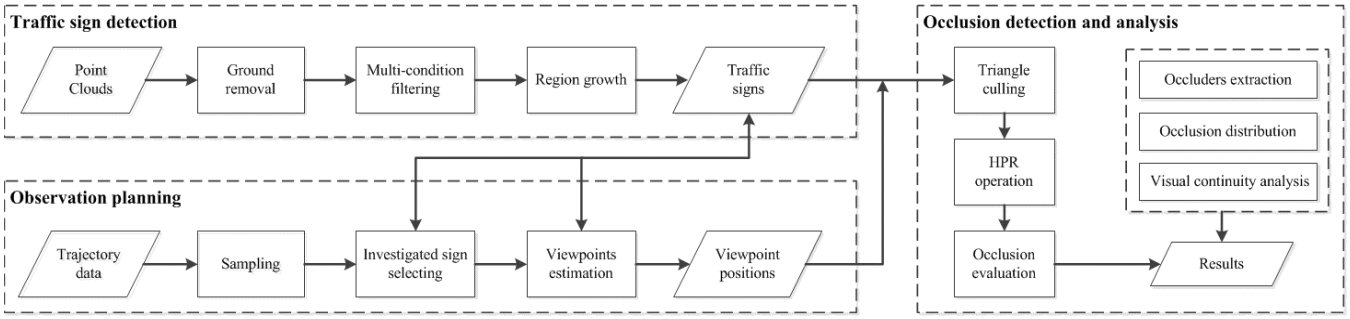

Fig. 2. Workflow of the proposed method.

(a) (b) (c) (d)

Fig. 3. The process of traffic sign detection: (a) raw point clouds, (b) ground removal, (c) traffic sign detection results, (d) the repaired results after region growth.

III. Methodology

To detect occlusions of traffic signs and analyze the degrees of the occlusions in real-world scenes, we propose a novel framework as shown in Fig. 2. Firstly, traffic signs are extracted from MLS point clouds with high integrity and accurate positioning information. Secondly, head-on traffic signs are selected from the extracted traffic signs based on trajectory data, and the viewpoints of drivers are estimated. The head-on traffic signs are those that locate in front of drivers and provide road information for drivers directly. After estimating the locations of drivers' viewpoints, an observation relationship between the observed traffic sign and the corresponding viewpoint is established. Finally, the hidden points of the traffic sign from the corresponding viewpoint are calculated by simulating the visual field. Based on the obtained hidden points, three indexes (occlusion percentage, occlusion distribution, and visual continuity of a traffic sign) are used to evaluate the occlusion degree of a traffic sign.

A. Traffic Sign Detection

Traffic sign detection in point clouds determines which points belong to signs. Two major characteristics must be considered during the sign detection: correctness and completeness. Correctness is measured by the percentage of right detection points with respect to total points in a sign, which is important to our framework because extracting non-sign points increases false alarms. As for completeness, it requires that there are no missing points when the sign is extracted. The proposed sign detection algorithm consists of three steps: ground removal, multi-condition filtering, and region growth.

1) Ground Removal: Traffic signs are off-ground objects. Ground removal eliminates both ground points and various roadblocks from the point clouds. To improve the processing efficiency of our framework, as well as avoid the interference of road marking to sign detection, a voxel-based ground removal algorithm [21] is adopted to extract off-ground points. Fig. 3 (a) and (b) show MLS raw point clouds of road scene and the results of ground removal, respectively. As we can see, the traffic signs are contained in off-ground points.

2) Multi-Condition Filtering: The objective of multi-condition filtering is to ensure sign point detection as accurate as possible. The reflectivity of traffic signs' surface material must meet stringent requirements (e.g., MUTCD [22]) to ensure visibility in all-weather conditions. In laser scanning point clouds, an object's surface with high-reflectivity has a significantly higher intensity value than others, which is one general characteristic of various laser scanners [9], [19], [20]. In this paper, an intensity filter is used to select suspected traffic sign points at first. The points with an intensity value greater than the intensity threshold ω_c are labeled as suspected sign points and remained for further processing. The traffic sign board (or panel) on the opposite direction of driving is ignored after intensity filtering because there is no reflective material on the back of signs.

After intensity filtering, the clustering operation is implemented for the following object-oriented filtering. We use an Euclidean distance clustering algorithm to cluster the remained points into several suspected traffic sign objects and compute the center of each cluster as c, $c=[x_c, y_c, z_c]^T$. Then, the typical sizes of traffic signs are used to remove small objects (e.g., license plates, guideposts, and road blocks). An object will be removed if the height of the object is smaller than Z_c or the number of points in the object is less than N_c. In addition, considering that a traffic sign is a flat object, we propose a shape-based filtering to exclude the pole-like objects (e.g., traffic sign poles or balusters). First, by using a principal

component analysis based method [23], we obtain Eigen-values $\lambda_0, \lambda_1, \lambda_2$ and Eigen-vectors e_0, e_1, e_2 with regard to the whole object point set. Then, a narrow degree (or aspect ratio) of a plane is defined as the ratio of secondary direction length to principal direction length, and can be approximately computed by $\lambda_1 \big/ \lambda_0$. If an object's narrow degree is smaller than the threshold S_c, the object is removed. The remaining objects are recognized as traffic signs. Fig. 3(c) shows the correctly detected traffic signs, in which each sign was painted a color different from the pseudo-color background.

3) Region Growth: Due to attenuation of the reflectance (e.g., retro-reflective material aging), some points in the traffic sign objects are missing as shown in the boxes in Fig. 3(c). Therefore, a region growth algorithm is used to retrieve the missing points.

The rule of the growth is to find the points coplanar with a traffic sign within a sphere region and add the points to the sign. First, a sphere region centered at the sign's clustering center is specified to delimit the growth area. Let d_{max} be the distance between the clustering center c and the furthest point in the cluster, and α is a magnification factor with $\alpha > 1$ to keep the region large enough to cover the sign. The growth region Ω is a subset of the raw point set given by:

$$\Omega = \{p \mid \|p - c\| \leq r, r = \alpha d_{max}\} \tag{1}$$

where $\|\cdot\|$ is the norm operation. Then, for each point $\in \Omega$, we calculate the unit normal vector e_2 and the Eigen-based local geometry at p [24]. The radius of the neighborhood is 0.1 meter (m), which is recommended in [25]. During the growth, the points in the cluster serve as the original seed points. Suppose $q \in \Omega$ is a non-sign point and s is one of its neighboring seed points, and let $e_{2,q}$ and $e_{2,s}$ be the normal vectors at q and s respectively, if the dot product of $e_{2,q}$ and $e_{2,s}$ is greater than a threshold T_n, the non-sign point q is added to the sign points. Furthermore, if a newly added point satisfies:

$$\begin{cases} \sigma_0 \Big/ \sum_{i=0}^{2} \sigma_i < 0.6 \\ \sigma_2 \Big/ \sum_{i=0}^{2} \sigma_i < 0.2 \end{cases} \tag{2}$$

where $\sigma_i = \sqrt{\lambda_i}$, $i = 0, 1, 2$, which indicates the point is not on the edge or thickness part of the plane, the point is used as the new seed point. After region growth, the clustering center c and the set of the sign points are used for the following head-on traffic sign selection and occlusion detection. Fig. 3(d) shows the traffic sign extraction results after region growth. Compared with Fig. 3(c), the results in Fig. 3(d) are more complete. The images within the colored boxes show the backsides of the traffic signs, which indicate that the pole points are excluded from the extraction results.

B. Observation Planning

The viewpoint indicates the position of the driver's eyes for observation. Correct spatial relationship between the viewpoint and the traffic sign is crucial to simulate the visual effect of the traffic sign from the driver's perspective. However, direct estimation of a driver's position is difficult, because environmental information (e.g., traffic area, terrain slope, and observation direction) is hard to obtain from unorganized point clouds. On the other hand, the trajectory information contains the vehicle's actual position, which is recorded at regular intervals (e.g., every 5 milliseconds in RIEGL VMX-450). The trajectory is obtained by the position and orientation system (POS), and is provided by all MLS systems. Thus, we propose a trajectory-based method which uses horizontal coordinates and time values of trajectory points to estimate viewpoints. Note that the elevation values of trajectory points are not considered in the calculation of observation planning. Since the road in this study is wide and flat, the locations on the driver's route and the traffic signs can be mapped and represented on a horizontal plane. Exclusion of the elevation value helps to simplify our calculation and prevent high hanging traffic signs from being ignored in observation planning. Furthermore, we select the traffic signs located ahead of the vehicle according to the heading direction of the trajectory.

First, trajectory points are uniformly sampled to reduce the number of possible viewpoints. Then, for selecting the traffic signs to be observed, we create a KD-tree index structure for trajectory points. For each traffic sign, the horizontal coordinates of the center $\hat{c}$, $\hat{c} = [x_c, y_c]^T$, is set as a query point. We find the nearest trajectory point v_n from the query point $\hat{c}$ to create an observation vector, indicating potential observation direction of the driver. Furthermore, to create motion vector of the driver, we compute the mean coordinates v_m of several forward trajectory points, whose time values are greater than that of v_n. Thus, to determine the traffic sign in question is on the driver's right or left, the cross product of the motion vector and the observation vector is calculated as follow:

$$v_s = (v_m - v_n) \otimes \left(\hat{c} - v_n\right) \tag{3}$$

where $\otimes$ is the cross product operator. If the direction of v_s is opposite to Z axis, the traffic sign is on the trajectory's right side. Let z_s be the z-coordinate of v_s, to select the traffic signs that the driver should observe, a decision function is defined as follow:

$$f\left(\hat{c}\right) = \begin{cases} 1 & \left\|\hat{c} - v_n\right\| < T_r \ \ \& \ \ z_s \leq 0 \\ 1 & \left\|\hat{c} - v_n\right\| < T_l \ \ \& \ \ z_s > 0 \\ 0 & otherwise \end{cases} \tag{4}$$

where $\left\|\hat{c} - v_n\right\|$ indicates how far the sign is from the route. It is also a minimum offset from the path to help determine a road's boundaries [26]. T_r and T_l are right and left distance thresholds respectively. A traffic sign with $f\left(\hat{c}\right) = 0$ degrades to background.

The next step is to put viewpoints in right places to build a continuous observation relationship for the remaining traffic signs. The minimum requirement for traffic sign's working area, L_m, is used as the maximum distance of visibility survey to locate the farthest viewpoint. Thus, for a selected traffic sign, the section of trajectory between the nearest and farthest points is considered the observation interval (the colored lines in Fig. 4(a), each for a traffic sign with the same color). Finally, the trajectory points in the farthest two-thirds parts of the observation interval form normal observation angles for the driver, comprising a strand of viewpoints.

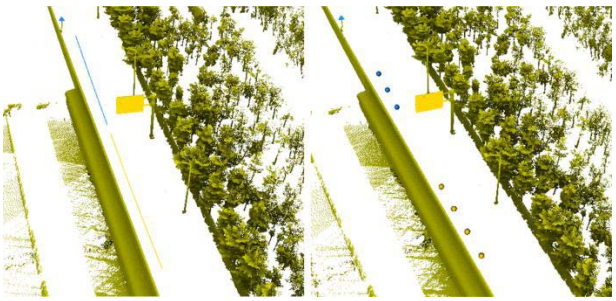

Fig. 4. Viewpoints estimation for two traffic signs: (a) observation interval of traffic sign, (b) estimated viewpoints.

We use the trajectory's original elevation values (z-coordinates) to simulate the heights of a truck driver's eyes. For different vehicle type, an appropriate offset should be added to original elevation values to rectify the heights of the viewpoints. Fig. 4(b) shows that the viewpoints are correctly located at the driver's actual positions.

C. Occlusion Detection and Analysis

1) Occlusion Detection: A viewpoint will act as an observer (driver) and an observation relationship is established between the viewpoint and the traffic sign to detect if an occlusion exists. For each viewpoint, to simulate the driver's view as well as to reduce the computation cost of occlusion detection, the points belonging to field of view (FOV) is segmented by view frustum culling first.

In fact, data volume in vertical direction of the view filed is small, because the ground points under the traffic sign have been removed. Thus, the view frustum is replaced by a simple triangle model on a horizontal plane to avoid redundant computations.

Each traffic sign is limited to a spherical region Ω. Therefore, the solution is equivalent to generate, on a horizontal plane, a circle containing the whole traffic sign and an isosceles triangle inscribing the circle. As shown in Fig. 5(a), vertex $\hat{p}_v = [x_v, y_v]^T$ is the horizontal location of the viewpoint, and $\hat{c}$ is the horizontal center of the target traffic sign. The perpendicular bisector through $\hat{p}_v$ and $\hat{c}$ has a length $l + r$, where l is the distance between $\hat{p}_v$ and $\hat{c}$: $l = \left\| \hat{p}_v - \hat{c} \right\|$. The radius r of the spherical region Ω in (1) is added to extend the perpendicular bisector for determining the far clipping plane. Let d be half of the length of the base of the isosceles triangle, determined as follow:

$$d = (l + r)\, tan\left(arcsin\left(r/l\right)\right). \tag{5}$$

If $r/l \geq 1$, the viewpoint $\hat{p}_v$ is near or below the traffic sign and is not considered in occlusion detection.

After establishing the triangular field of vision from a viewpoint to a traffic sign, the culling operation determines which points are inside the triangular area. The off-ground points are tested one-by-one via the Barycentric Coordinates method, and the inside points are extracted for further occlusion analysis. In Figs. 5(c) and (d), the colored points (green or red) are inside points, and the grey points lie outside the visual field.

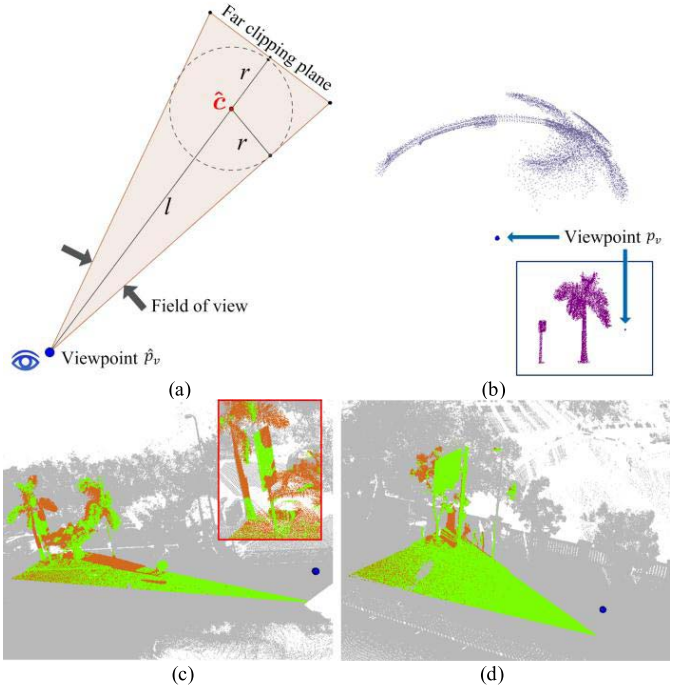

Fig. 5. The occlusion detection for traffic signs: (a) the field of view demarcation, (b) 3D spherical inversion, (c) and (d) the view analysis result of traffic signs in point clouds.

The visibility determination in polygons form [27] (e.g., triangles model) requires modeling of point cloud object, and no doubt it would magnify the problem that we already face. Alternatively, the hidden point removal (HPR) operator proposed by Katz *et al.* [28] and developed by Mehra *et al.* [29] determines point visibility requiring no preprocessing in raw point clouds, which is used in our method. The algorithm is also used as a visual comprehension-based method to reduce point cloud data [30]. Considering the points of view field as an inspected 3D point set P, and a driver's viewpoint $p_v = [x_v, y_v, z_v]^T$ as the query viewpoint, we apply the HPR operator to estimate which points are hidden from the visual field. The HPR operator starts with the spherical inversion shown in Fig. 5(b). For point set P, a sphere centered at viewpoint p_v (which is reset to the origin in local coordinates) is supposed to contain all of points p_i, $p_i \in P$ (purple points in the box). The radius of the sphere R_h is according to the maximum distance from the viewpoint to the point set of view field. Then, through being projected out of the sphere along a ray from the sphere's center, each point p_i attains a new position $\breve{p}_i$ (black point in Fig. 5(b)):

$$\breve{p}_i = f_h\left(p_i\right) = p_i + 2\frac{p_i}{\|p_i\|}\left(R_h - \|p_i\|\right) \tag{6}$$

where f_h is a spherical inversion function with a mirror kernel [31]. Based on the inversion function, points adjacent to viewpoint p_v are inverted to a far position, i.e., they are transformed to the surface of the sphere. Thus, a 3D convex hull is constructed to surround the point set $\breve{P} \bigcup \{p_v\}$, where $\breve{P}$ is the point set of view field after inversion. Finally, the points on the surface of the convex hull are determined as visible points, and the points within the convex hull will be

hidden from the viewpoint. As shown in Figs. 5(c) and 5(d), the red points are the occluded part from the viewpoint, and the green points are the visible part. The traffic sign in Fig. 5(c) is partly occluded, and the one in Fig. 5(d) is completely visible.

Considering the traffic sign point set G, $G \subseteq P$, and the view field's hidden point set H, $H \subseteq P$, the traffic sign hidden point set is $\tilde{P} = G \bigcap H$. The occlusion degree is measured by a center distance weighting function to estimate the effective information loss level:

$$f_o\left(\tilde{P}\right) = 1 - \frac{1}{m}\sum_{i=1}^{n}\left(1 - \varphi\frac{\|\tilde{p}_i - c\|}{r}\right) \tag{7}$$

where $\tilde{p}_i \in \tilde{P}$, m and n are the cardinalities of G and $\tilde{P}$ respectively, and φ is the distance weight factor.

An occlusion should be recorded even if only the boundary points of the traffic sign are hidden, since the degree of occlusion may worsen with plant growth. Thus, we use $\varphi = 0$ in (7), denoting the number of hidden points in the traffic sign point set, to judge occlusion. If the function's value is less than an alarm value T_a from any one of the viewpoints, the observed traffic sign is considered to be occluded.

2) Occlusion Analysis: After occlusion detection, a ray tracing method is proposed to obtain the occluder of a traffic sign. The occluder is made of the points in the view field that occlude the driver. A general idea is that the occluder surface intersects the ray from driver's viewpoint to the points of the traffic sign in occlusion. Based on the previous steps, for each viewpoint p_v, we have an occlusion point set of the traffic sign as $\tilde{P}$, $\tilde{P} = \{\tilde{p}_i \mid i = 1,2,\ldots,n\}$, where n is the cardinality of the point set (empty set for a clear view). As such, a searching method, which finds points near the ray instead of judgment intersection, is implemented. If the distance d_o from a query point p_j ($p_j \in P$) to that ray is smaller than ρ, it will be considered as an occluder point, where ρ is the density of point clouds. The distance d_o can be computed by $d_o = \left\|p_v - p_j\right\| sin < p_v - \tilde{p}_i, p_v - p_j >$, which is equivalent to $d_o = \left\|(p_v - p_j) \otimes (p_v - \tilde{p}_i)\right\| \big/ \|p_v - \tilde{p}_i\|$. Besides, the point should simultaneously satisfy $\left\|p_v - p_j\right\|^2 - d_o^2 \leq \|p_v - \tilde{p}_i\|^2$ and $\left\|\tilde{p}_i - p_j\right\|^2 - d_o^2 \leq \|p_v - \tilde{p}_i\|^2$ in order to assure that the occluder point is located between the viewpoint and the traffic sign. Based on the prior knowledge provided by view field point set P, these conditions can be transformed as simple as $v_{tv}v_{tj} > 0$, where $v_{tv} = (p_f - c) \otimes (p_v - c)$ and $v_{tj} = (p_f - c) \otimes (p_j - c)$; c and p_f are the center point and the farthest point of the current traffic sign respectively. Note that this computation is on a horizontal plane.

To further our quantitative analysis, we propose two indexes to help evaluate the occlusion of a traffic sign. 1) The occlusion distribution index D_d and 2) the occlusion gradient index D_g. The occlusion distribution index shows the severity of occlusion through measuring the distribution of occluded points on the traffic sign surface. The index function is expressed below:

$$D_d = \frac{1}{n}\sum_{i=1}^{n} exp\left(-\frac{K\|\tilde{p}_i - c\|^2}{2\left\|p_f - c\right\|^2}\right) \tag{8}$$

where $D_d \in (0, 1]$, n is the cardinality of $\tilde{P}$. The value of the index is higher when the occlusion is closer to the center of the traffic sign, where the sign text likely is located. The parameter $K = -8\ln(1/2)$ to make sure $D_d = 1/2$ when $\|\tilde{p}_i - c\| = \left\|p_f - c\right\|/2$. The occlusion gradient index measures the visual continuity of a traffic sign during driving, i.e., how fast a traffic sign either moves away from or moves into an occluder, thus showing whether the traffic sign is in a complex environment, where the driver may have to pay more attention to navigate through. We use a first difference operator to describe the variation rate of occlusion evaluation function as $\Delta F(f_o(\tilde{P}_k)) = f_o(\tilde{P}_k) - f_o(\tilde{P}_{k+1})$, $k \in [1, 2, \ldots, s-1]$, s is the number of viewpoints. Thus the occlusion gradient index is established below:

$$D_g = max\,\Delta F(f_o(\tilde{P}_k)) \tag{9}$$

where $D_g \in [0, 1]$. The greater the observation changes, the higher the value of D_g becomes, which can then be used to judge whether the occlusion risk can be tolerated.

IV. Results and Discussion

A. Device and Datasets

The study data were acquired by RIEGL VMX-450 and included two datasets. The accuracy and precision of VMX-450 are 8 millimeters (mm) and 5 mm, respectively. The measurement rate used is 760 kHz with a 330 m measurement range. The point density of data sets is about 3,855 points/m^2 for the ground area around the trajectory. The system implements 360° seamless scanning, see more detailed function introduction in [32]. VMX-450 can also record trajectory data with accurate position and attitude in WGS84, and the relative positioning precision is 10 mm. Thus, the preprocessing of our system only needs to convert each point from WGS84 to UTM and elevation that are used as relative coordinates, which is also auto-completed by VMX-450. All the calculations can be conducted in relative coordinates. This paper utilized both raw 3D point clouds data with intensity and raw trajectory points with time records.

The first dataset (Dataset I) was obtained from a survey of Island Ring Road, Xiamen, China, conducted in November 2013. The Island Ring Road is representative of diverse traffic scenes that include a bridge, a residential area, and a tunnel. Besides, lining along the street are many tropical trees that obscure the traffic signs. The second dataset (Dataset II) was acquired in Dongdu, Xiamen, in June 2015. Investigated scenes in Dataset II include Haicang Bridge, a junction with heavy traffic. There is less vegetation on both sides of the road. The RIEGL VMX-450 system was mounted on a multi-purpose Buick Terraza minivan, and data were acquired at a normal speed.

Dataset I consisted of more than 1.07 billion points with a data size of 33.92 GB, and Dataset II was up to 13.46 GB including 0.43 billion points. In the actual processing, rather than as a single input, Datasets I and II were divided into 67 packets and 45 packets respectively, to prevent excessive loading. The maximum number of points in one data packet was about 30.15 million in Dataset I and 38.30 million in Dataset II. The total distances of the surveyed roads L_t were about 13.85 km as represented by Dataset I and 9.83 km

TABLE I
PARAMETERS USED IN THIS STUDY (DATASET II/DATASET I)

Parameter	Traffic sign detection					Observation planning			Occlusion detection
	ω_c	Z_c (m)	N_c	S_c	T_n	T_r (m)	T_l (m)	L_m (m)	T_a
Value	0.85	0.50	100/200	0.05/0.1	0.99	15.00	3.50	25.00	0.90

TABLE II
COMPUTING TIME

Dataset	Steps			Total costs (min)	Average costs (min/km)
	Traffic sign detection (min)	Observation planning (s)	Occlusion detection (min)		
I	288.68	0.11	491.89	780.57	56.36
II	67.27	0.02	283.89	351.16	35.72

by Dataset II. The distances were determined from survey distance statistics which were derived from the trajectory data.

B. Results

Before execution of the algorithm, the aforementioned important parameters are shown in Table I. Parameters Z_c, T_l, T_r, and L_m can be determined directly based on the local traffic facility construction standards. Z_c is set based on the minimum traffic panel height. T_l and T_r are set based on the road width, T_l is suggested to be the one-lane width. L_m is set based on the safe sight distance according to the local laws and regulations. ω_c is set to be a fixed value since the intensity ranges of point clouds are normalized. To adapt to the specific parts of the two data sets, S_c is set to be a larger value in downtown (Dataset I) to eliminate street name plates, which are irrelevant to this experiment. N_c is set to be a smaller value in Dataset II due to the data density. As N_c, S_c and T_a are set empirically, an impact analysis for these 3 parameters will be presented later on.

The developed algorithm was coded in C++ and ran on a personal computer, configured with an Intel(R) Core(TM) i5-3470 CPU 3.2 GHz and a RAM 16.0 GB. As shown in Table II, run in debug model, the total time required for processing the experimental datasets was 1131.73 minutes, mostly consumed on occlusion detection. Even with the measurement of multi-viewpoints in a large scene, the average time for a single traffic sign analysis was less 3.82 minutes. To further verify computation speed, our traffic sign detection method and [19] are run under the release model. For a 22.27 GB dataset with 8.49 km long urban scene, computation times of our paper and [19] are 6.04 and 5.95 minutes, respectively. In essence, the processing speed of our method is very close to [19] and should be sufficient for the off-line system. To avoid redundant computation, the procedure for traffic sign detection was restricted to a narrow range of the traffic sign region. Increasing the number of points and densities also increases the burden of traveling and computing. In particular, sections of a congested region (e.g., downtown) produce high density point clouds and dense viewpoints. Hence, data acquisition is better conducted when the traffic is light. If it is necessary to speed up processing, the down-sampling operation may be performed after collecting data.

To quantitatively evaluate result, for traffic sign detection, the position and number of traffic signs in each point cloud data patch is manually checked and labeled as ground truth. For observation planning, we check and label which traffic signs should be noticed by driver, which are carried out by examining the image data acquired by the VMX-450 and Baidu Street View. The image data are also used as reference data in occlusion detection. The Baidu Street View enables the user to obtain road scene images of interest and provides the street view information. For occlusion detection, we manually check the visibility of an observed traffic sign at the viewpoint system returns. Note that a traffic sign is labeled as occluded traffic sign as soon as occlusion is regarded to have taken place at anywhere within the given viewpoints. In the two datasets, there were 274 targeted traffic signs that a driver might need to pay attention to. However, for our method it was not necessary to detect superfluous traffic signs, e.g., those signs that are contra flow or far from the roadway. On the other hand, U-turn traffic signs were included as targeted traffic signs even when the driver was traveling straight on and outside the turning lane. Only two targeted traffic signs lost during collection, which indicated the high data integrity of point clouds. To quantitatively analyze results and error propagation in each step, we used the F1-measure to estimate our results of traffic sign detection and viewpoint selection. F1-measure F_1 is dependent on precision P and recall R. For computing those two indexes above, the true positives (TP), false positives (FP), false negatives (FN), and true negatives (TN), are defined as follows.

1) Traffic Sign Detection: For traffic sign detection, TP indicates the correct detection of targeted traffic signs, whereas FP means that non-traffic sign objects were detected from the background by mistake. FN indicates the missed detection of targeted traffic signs. Traffic sign detection results were shown in Table III. Almost all of the traffic signs were completely retained in the results, as only a few signs were not

TABLE III
THE TRAFFIC SIGN DETECTION RESULT OF EXPERIMENTAL DATASETS

Items	Dataset	TP	FP	FN	Precision (%)	Recall (%)	F1-measure (%)
Traffic sign detection	I	165	15	4	91.67	97.63	94.56
		Number of errors per kilometer (E_k): 1.37					
	II	101	7	4	93.52	96.19	94.84
		Number of errors per kilometer (E_k): 1.12					

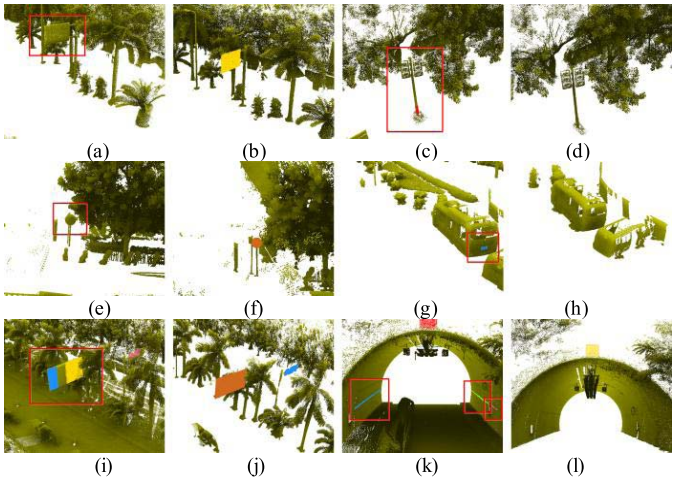

Fig. 6. Comparison of four traffic sign detection methods: (top to bottom row) the illustrated detection results by method [9], [19], and [20], respectively, (the first and third columns) the false negative and false positive results by the corresponding methods, (the second and fourth columns) the detection results by our method.

detected because their intensity values were missing or due to abnormal shape stenosis. False positive objects include high reflective billboards and huge traffic poles. Because occluded traffic signs usually are covered and thus lose structure in the data, a strict filtering would improve precision but potentially lose occluded traffic signs. Thus, our approach is to sacrifice some precision for higher recall. To add more significant features will be helpful for reducing false positives. In other words, even if there were no traffic signs on some road sections, our algorithm was still tested continuously in varying surroundings. Hence, an evaluation index term E_k, indicating the number of errors per kilometer ($E_k = (FN + FP)/L_t$), was proposed. The values of E_k were calculated to be less than 1.37 in Dataset I and 1.12 in Dataset II, which were satisfactory for a practical application. The low error rate was attributed to vigorous filtering of suspected objects.

To quantitatively analyze the suitability of our detection method for applying to the traffic sign occlusion system, we compared our method with three typical methods: a pole based method [9], a data attributes based method [19] and a trajectory based method [20]. Half of the Dataset I, including 84 targeted objects, were used in the comparison experiments. Table IV indicates that our proposed method has a higher recall, which means it would miss fewer traffic signs, thus meeting the high recall requirement of an occlusion detection system. Fig. 6 shows the false traffic sign detection results of the three contrasting methods. Fig. 6 (a) and Fig. 6 (c) show FN and FP cases of the method in [9], respectively.

TABLE IV
QUANTITATIVE RESULT OF COMPARED EXPERIMENTS IN TRAFFIC SIGN DETECTION

Method	Our method	Wen's method [9]	Chen's method [19]	Ai's method [20]
TP	82	78	79	75
FN	2	6	5	9
FP	7	7	16	4
Precision (%)	92.13	91.76	83.16	94.94
Recall (%)	97.62	92.86	94.05	89.29
F1-measure (%)	94.80	92.31	88.27	92.02

Using PCA method to judge a linear structure in [9] may not be able to deal with a huge pole or pole structure loss. With regard to the method in [19], in downtown area there are a lot of traffic signs that are parallel to the road (e.g., no parking sign shown in (e)), which increases FN. Small reflective objects on the road also increase the FP of this method, as shown in (g). Figs. (i) and (k) show the FN and FP cases of the method in [20], respectively. Utilizing trajectories to remove reflectors on the road in [20] may inadvertently remove or split overhead traffic signs. (d), (h) and (l) show that our method survived from interferences by the same high reflective objects (e.g., linear objects and small objects). Our F1-value of 94.80% benefited from the targeted filtering of reflectors, which demonstrates the advantage of our method. Besides, rather than removing local outliers, our method using the region growth operation maintains the completeness of traffic signs for further visibility analysis.

2) Observation Planning: For observation planning, TP indicates that the correct observation model is established between the traffic sign board observed by drivers and the corresponding observation viewpoints. FN indicates that the traffic sign has not been observed by the system; FP signifies that a false observation model is set up between the viewpoint and some irrelevant traffic sign. For example, due to the complexity of an urban traffic environment, a traffic sign may physically appear ahead of the driver, but it is intended for the traffic in the opposite direction and thus is regarded as irrelevant to the concerned driver. As shown in Table V, the F1-value of two datasets for traffic signs and viewpoint selection are all 93%. Traffic signs on the right side of the roadway and panels above the roadway were easily detected among the observed objects. False negative traffic signs were mostly U-turn signs, which were usually placed in the left

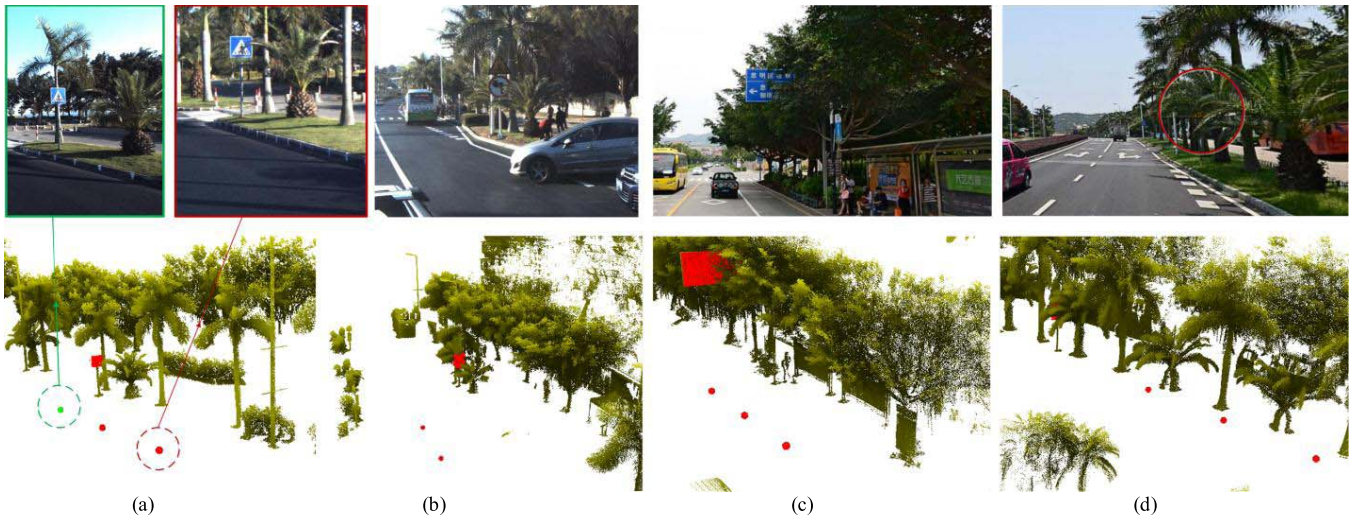

Fig. 7. Occlusion detection of traffic signs in different obscured extent: (top line) the true situation of traffic signs, (bottom line) the detection results of our occlusion detection method.

TABLE V
THE HEAD-ON (OBSERVED) TRAFFIC SIGN SELECTION RESULT OF EXPERIMENTAL DATASETS

Items	Dataset	TP	FP	FN	Precision (%)	Recall (%)	F1-measure (%)
Traffic sign selection	I	151	8	14	94.97	91.52	93.21
	II	89	1	12	98.89	88.12	93.19

and away from the straight line and the direction of travel. Strict trajectory control can solve this problem. As shown in Fig. 7, according to the traffic-sign-based search method, viewpoints were correctly placed for driver observation and the oncoming viewpoints were rapidly extracted automatically. To deal with complex scenes, the multi-viewpoint measure mode made the traffic occlusion analysis more dynamic, specific, and controllable.

3) Occlusion Detection and Analysis: For occlusion detection, the detection is equivalent to a binary classification result of traffic sign visibility, i.e., occluded or visible. TP represents the number of traffic signs that actually have been covered by our method in any obstructed viewpoints and alerted as an occlusion. Any alarm of a viewpoint indicates the traffic sign is confusing the driver. FP means that false occlusion alarms are produced for visible traffic signs. Conversely, TN is the actual visible traffic sign in clear view without any alarm. FN denotes that our method did not correctly detect the occluded traffic signs. In this paper, any alarm of viewpoints that led to confirm the corresponding traffic sign occlusion, we manually checked the ground truth by an approximate distance threshold as the criteria to judge that the object was occluded. In addition, in view of the imbalance Dataset II, an overall accuracy rate (ACC) was added to evaluate both occlusion and clarity.

With the procedure of traffic sign detection and viewpoint selection, 240 traffic signs were selected, in which 44 obscured traffic signs and 180 clear traffic signs were correctly detected. The results show that a survey section along a scenic spot with dense tropical plants will produce a large number of actual occluded traffic signs. We believe a 25 m safe distance is too restrictive for traffic signs in certain localities (e.g., urban centers), where it is difficult to maintain an ideal distance between road facilities because of the positioning of the traffic signs and the shortage of urban spatial resources. To detect occlusion in a downtown area, we suggest a shorter viewing distance. As shown in Table VI, FP and FN are suppressed over all data. For occluded traffic signs, an average recall of 91% is obtained. F1-measure value of Dataset II dive is due to data imbalance. The high recall means that the system detected almost all of the occlusions. For the overall evaluations, the ACC of two datasets was 93%, demonstrating the analysis reliability on both classes of objects.

In order to further evaluate the system, four traffic signs with different degrees of occlusion are illustrated in Fig. 7. Figs. 7(a) to 7(d) show traffic signs that are slightly occluded, partially occluded, seriously occluded, and fully occluded, respectively. For the slightly occluded traffic sign in Fig. 7(a), our proposed system quantitatively analyzes and labels corresponding visibility results from different positions. The real situation (in red box) shows that the traffic sign is obscured by the cycad branches; the green box shows a clear view of the traffic sign after the driver has passed by the obstructing plant. The severe occlusion in Fig. 7(c) and full occlusion in Fig. 7(d) demonstrate our method's detection capability in extreme cases. A view detection method must deal with the challenges of the complex road background, and that is why the salient intensity features are taken as the initial clues for detection.

In the error analysis of occlusion, for FP, one of major reasons that occlusion analysis results exceed the alarm threshold is that the extracted traffic sign contained the pole points that

TABLE VI
THE OCCLUSION DETECTION RESULT OF EXPERIMENTAL DATASETS

Dataset	TP	FP	FN	TN	Precision (%)	**Recall** (%)	F1-measure (%)	**ACC** (%)
I	35	7	3	106	83.33	**92.11**	87.50	**93.38**
II	9	5	1	74	64.29	**90.00**	75.00	**93.26**

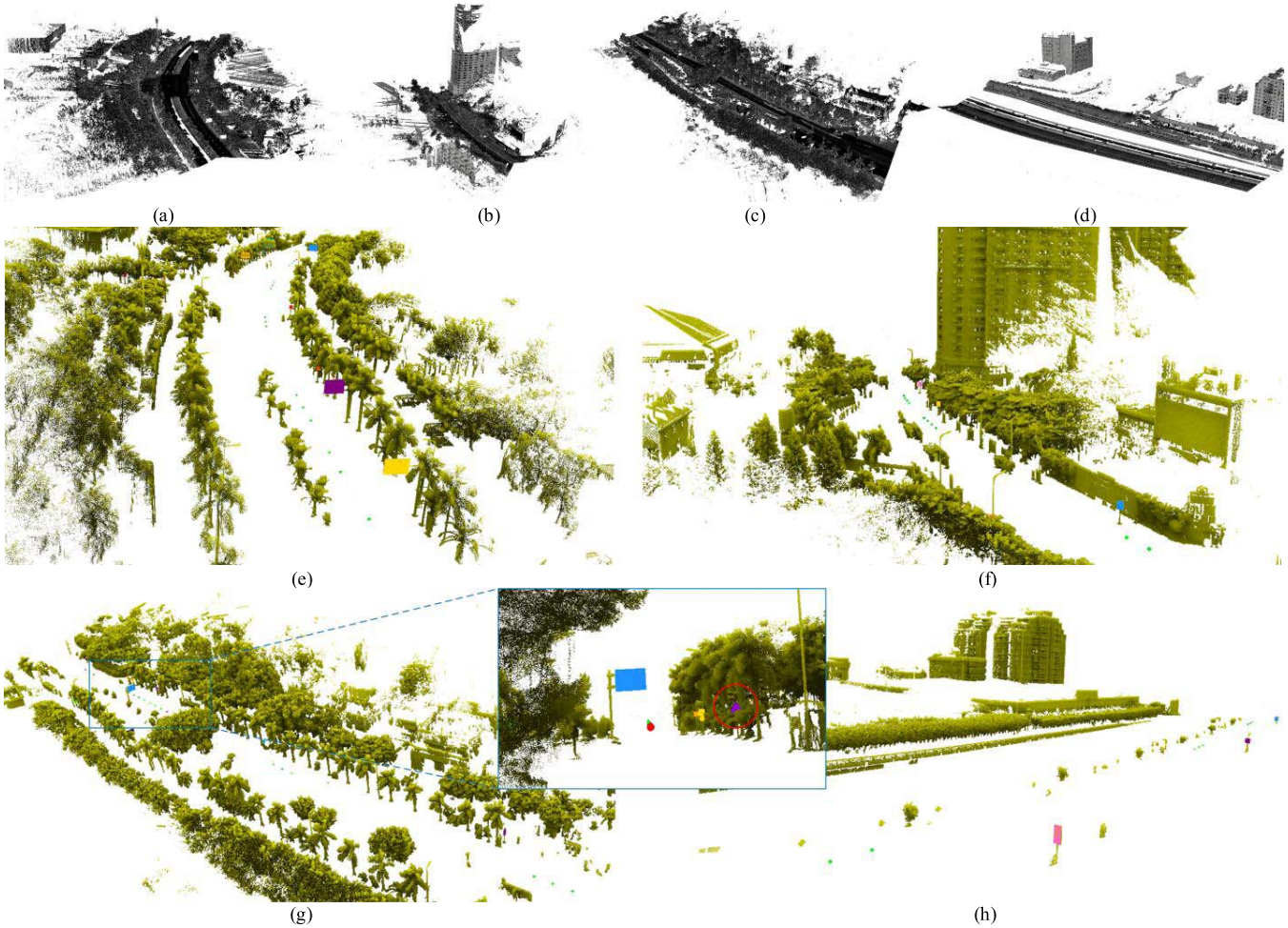

Fig. 8. Occlusion analysis results: (a), (b), (c) and (d) four raw MLS point clouds; (e), (f), (g), (h) closed view of the occlusion analysis results of (a), (b), (c) and (d), respectively. (Driver viewpoints are marked as green ball for clear view and red ball for obstructed view).

were partially occluded. The FP rose was also caused by being occluded by passing bus. One case of occlusion was due to a data error. Setting a low alarm threshold can reduce the false alarm rate. However, compared to a FP monitoring error, traffic safety is more important and thus our method was designed to be more sensitive to occlusion. For FN, all four cases appeared to be large traffic signage panels with partial occlusions that registered below the alarm threshold. It is quite reasonable that large area panels would tolerate a greater amount of intrusion from vegetation.

Finally, of the 274 targeted traffic signs in ground truth, 224 were exactly and correctly detected, located, and analyzed in each step of our method. The statistic results in each step revealed that the precision (%) and recall (%) in Dataset I was 82.46 and 87.04, in Dataset II was 86.46 and 83.00. Hence, the F1-value (%) with an overall result of 84.68 for Dataset I and 84.69 for Dataset II was obtained under the evaluation by our method. As shown in Fig. 8, our method performed well in various scenes (Figs. 8(a) and 8(b) downtown; Fig. 8(c) scenic area and Fig. 8(d) bridge), demonstrating its powerful traffic sign detection and analysis ability that meets the requirement for traffic sign maintenance. As a result of the survey, each detected traffic sign was painted with a different color; viewpoints were correctly located and colored either green (for clarity) or red (for occlusion). The coordinates of a red viewpoint and its observed traffic sign were recorded. Several video results of our method are available at http://rssi.xmu.edu.cn/publications/videos.rar. The main cause of performance degradation was false traffic signs and missing observation targets that were too far away from a straight lane. Adding more location data may improve the performance. We believe that conducting data collection at midnight

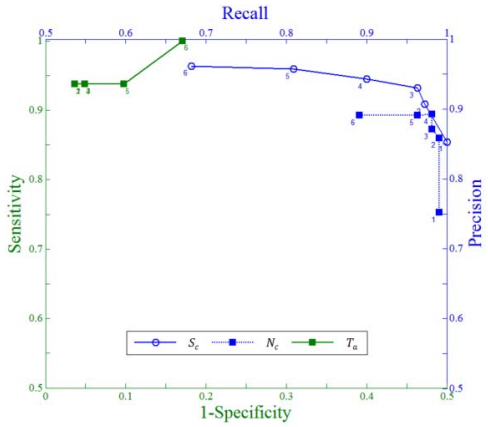

Fig. 9. Impact of parameters N_c, S_c and T_a.

(with little traffic) would be better for controlling the trajectory and avoiding vehicle occlusion.

To analyze the impact of the parameters N_c, S_c and T_a, one third of two data set combination is used, including 38 randomly selected packets. For each parameter, we tested a sequence of 6 value configurations, as labeled from 1 to 6 (from the smallest value to the largest value) in Fig. 9. The impact of varying N_c and S_c is represented by precision-recall curves, shown in blue. N_c ranges from 40 to 340 with an interval of 60 ($S_c = 0.05$) and S_c ranges from 0.03 to 0.28 with an interval of 0.05 ($N_c = 100$). As seen, the precision quickly increases with $N_c \geq 100$ because the small reflective objects are removed. The recall decreases slowly when $S_c < 0.18$, indicating a smaller value of S_c is rather effective to distinguish linear objects from planar objects. To assure good performance, N_c and S_c are recommended to be set at 220 and 0.13, respectively. Due to data imbalance, the impact analysis of T_a is represented by receiver operator characteristic curve, shown in green. T_a ranges from 0.76 to 0.96 with an interval of 0.04 ($N_c = 100$, $S_c = 0.05$). In particular, the results do not show much changes as T_a increases from 0.76 to 0.80 and from 0.84 to 0.88. This is because that, relative to the sample distribution, the threshold set at these values is too relaxed. Thus, a threshold $T_a = 0.88$ should be enough in providing good performance that avoids interference from self-occlusion points.

In occlusion analysis, Fig. 10 shows three illustrated results of occluder extraction. The results present the points in the view field from the current viewpoint. The blue circle is the current viewpoint at the scene. In the images, the red points are the part of the traffic sign points which are in occlusion, and the blue points are the part of the traffic sign that can be seen from viewpoint, while the yellow points are the occluders from the viewpoint. The figures with blue borders show the results in a frontal view. As we can see, the occluders formed with various objects, e.g., leaves, tree trunks and light poles, have been extracted accurately.

Figs. 11(a) and (b) show different occlusion distributions on one object ($f_o = 0.66$ in (a) and $f_o = 0.72$ in (b)). In this case, the closer to the center the distribution gets, the greater the value becomes. Figs. 11(c) and (d) show two objects both with same occlusion percentage ($f_o = 0.73$ in (c) and

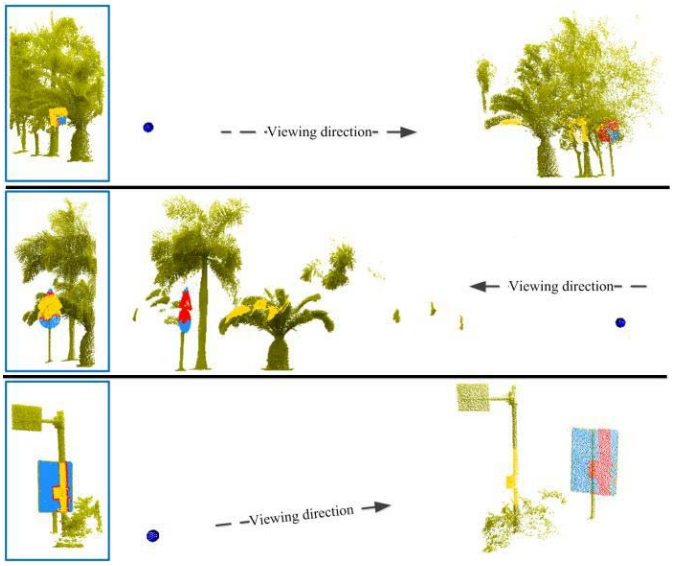

Fig. 10. Occluder extraction results. (Driver viewpoints are marked as blue ball).

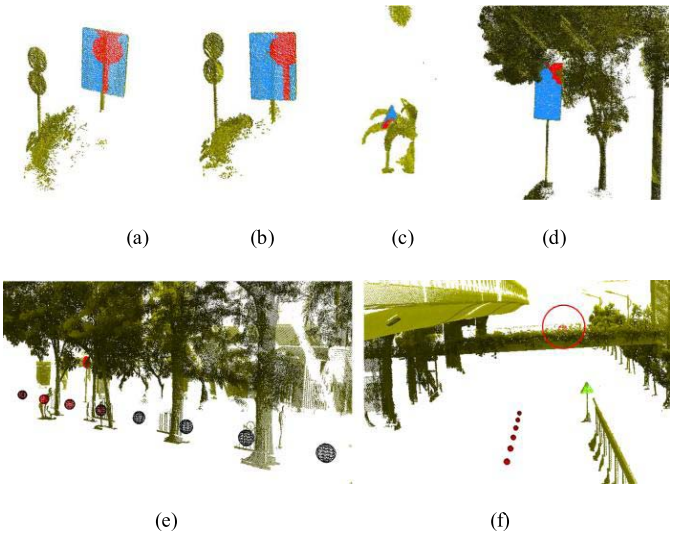

Fig. 11. The values of two proposed indexes: the distribution index in (a) $D_d = 0.57$, (b) $D_d = 0.44$, (c) $D_d = 0.55$, and (d) $D_d = 0.40$; the gradient index in (e) $D_g = 0.48$ and (f) $D_g = 0.09$.

$f_o = 0.76$ in (d)), but the traffic sign in (c) received more threat of occlusion and had a larger value of D_d. The results in Figs. 11(e) and (f) show the impact of complicated surroundings. The ball is colored from black to red (zero to max) to present the f_o value of each viewpoint. The driver had to pay more attention on the traffic sign in (e), even though cases (e) and (f) are both with serious occlusion. The result shows the traffic sign in (e) got a larger change (D_g), which could alert the traffic sign planner to relocate its position.

V. Conclusion

In this paper, we presented an automatic visibility inventory and survey method of traffic signs in MLS point clouds. The output of the method are geographic location of occluded traffic sign and observer (driver) with occlusion degree (i.e., percentage, distribution, complexity), and occluder points which provides guidance for road traffic sign maintenance.

There were no involvement with fitting, projecting, or modeling operations in proposed method, making it suitable for various scenes without a requirement for prior shape, color, and traffic sign placement attitude information. Experimental results demonstrate the feasibility of traffic sign occlusion detection in point clouds. Besides, our occlusion analysis approach in point clouds has wider potential in other traffic fields (e.g., traffic lights, billboards). The main obstacle to implementation lies in deciding the face points of target objects.

In the future, to reduce missing observations, we will focus on adding more geographic features to the head-on traffic sign selection model. Besides, as an offline system, our system can be speed up by multithreading processing or simultaneous processing of separated road sections. In addition, inspected objects will include, not only traffic signs existing in point cloud data, but also traffic signs designed through an interactive system. We believe this interactive system will effectively help traffic planners select the proper locations for new signs.

ACKNOWLEDGMENTS

The authors would like to thank Mike McAllister for his valuable assistance in proofreading this paper and Fukai Jia for his contribution in data collection.

REFERENCES

[1] (2003). *Law of the People's Republic of China on Road Traffic Safety, CHN*. [Online]. Available: http://www.gov.cn/english/laws/2005-09/07/content_29966.htm

[2] *Traffic Signs Manual*, 4th ed., U.K. Dept. Transp., London, U.K., 2013. [Online]. Available: https://www.gov.uk/government/uploads/system/uploads/attachment_data/file/226765/traffic-signs-manual-chapter-04.pdf

[3] A. Møgelmose, M. M. Trivedi, and T. B. Moeslund, "Vision-based traffic sign detection and analysis for intelligent driver assistance systems: Perspectives and survey," *IEEE Trans. Intell. Transp. Syst.*, vol. 13, no. 4, pp. 1484–1497, Dec. 2012.

[4] K. Doman *et al.*, "Estimation of traffic sign visibility toward smart driver assistance," in *Proc. IEEE IV*, Jun. 2010, pp. 45–50.

[5] Á. González, L. M. Bergasa, J. J. Yebes, and M. A. Sotelo, "Automatic information recognition of traffic panels using SIFT descriptors and HMMS," in *Proc. ITSC*, Sep. 2010, pp. 1289–1294.

[6] Á. González, L. M. Bergasa, and J. J. Yebes, "Text detection and recognition on traffic panels from street-level imagery using visual appearance," *IEEE Trans. Intell. Transp. Syst.*, vol. 15, no. 1, pp. 228–238, Feb. 2014.

[7] Á. González *et al.*, "Automatic traffic signs and panels inspection system using computer vision," *IEEE Trans. Intell. Transp. Syst.*, vol. 12, no. 2, pp. 485–499, Jun. 2011.

[8] E. Næsset and T. Økland, "Estimating tree height and tree crown properties using airborne scanning laser in a boreal nature reserve," *Remote Sens. Environ.*, vol. 79, no. 1, pp. 105–115, 2002.

[9] C. Wen *et al.*, "Spatial-related traffic sign inspection for inventory purposes using mobile laser scanning data," *IEEE Trans. Intell. Transp. Syst.*, vol. 17, no. 1, pp. 27–37, Jan. 2015.

[10] A. Golovinskiy, V. G. Kim, and T. Funkhouser, "Shape-based recognition of 3D point clouds in urban environments," in *Proc. IEEE ICCV*, Sep. 2009, pp. 2154–2161.

[11] Y. Yu, J. Li, H. Guan, and C. Wang, "Automated extraction of urban road facilities using mobile laser scanning data," *IEEE Trans. Intell. Transp. Syst.*, vol. 16, no. 4, pp. 2167–2181, Aug. 2015.

[12] B. Yang and Z. Dong, "A shape-based segmentation method for mobile laser scanning point clouds," *ISPRS J. Photogram. Remote Sens.*, vol. 81, pp. 19–30, Jul. 2013.

[13] B. Yang, Z. Dong, G. Zhao, and W. Dai, "Hierarchical extraction of urban objects from mobile laser scanning data," *ISPRS J. Photogram. Remote Sens.*, vol. 99, pp. 45–57, Jan. 2015.

[14] H. Wang *et al.*, "Object detection in terrestrial laser scanning point clouds based on Hough forest," *IEEE Geosci. Remote Sens. Lett.*, vol. 11, no. 10, pp. 1807–1811, Oct. 2014.

[15] M. Lehtomäki, A. Jaakkola, J. Hyyppä, A. Kukko, and H. Kaartinen, "Detection of vertical pole-like objects in a road environment using vehicle-based laser scanning data," *Remote Sens.*, vol. 2, no. 3, pp. 641–664, 2010.

[16] S. Pu, M. Rutzinger, G. Vosselman, and S. O. Elberink, "Recognizing basic structures from mobile laser scanning data for road inventory studies," *ISPRS J. Photogram. Remote Sens.*, vol. 66, no. 6, pp. S28–S39, 2011.

[17] H. Yokoyama, H. Date, S. Kanai, and H. Takeda, "Detection and classification of pole-like objects from mobile laser scanning data of urban environments," *Int. J. CAD/CAM*, vol. 13, no. 2, pp. 31–40, 2013.

[18] H. Gonzalez-Jorge, B. Riveiro, J. Armesto, and P. Arias, "Evaluation of road signs using radiometric and geometric data from terrestrial LiDAR," *Opt. Appl.*, vol. 43, no. 3, pp. 421–433, 2013.

[19] X. Chen, B. Kohlmeyer, M. Stroila, N. Alwar, R. Wang, and J. Bach, "Next generation map making: Geo-referenced ground-level LIDAR point clouds for automatic retro-reflective road feature extraction," in *Proc. ACM SIGSPATIAL*, 2009, pp. 488–491.

[20] C. Ai and Y.-C. Tsai, "Critical assessment of an enhanced traffic sign detection method using mobile LiDAR and INS technologies," *J. Transp. Eng.*, vol. 141, no. 5, p. 04014096, 2015.

[21] Y. Yu, J. Li, H. Guan, C. Wang, and J. Yu, "Semiautomated extraction street light poles from mobile LiDAR point-clouds," *IEEE Trans. Geosci. Remote Sens.*, vol. 53, no. 3, pp. 1374–1386, Mar. 2015.

[22] *Manual on Uniform Traffic Control Devices for Streets and Highways*, U.S. Dept. Transp. Federal Highway Admin., Washington, DC, USA, 2009

[23] J.-F. Lalonde, N. Vandapel, D. F. Huber, and M. Hebert, "Natural terrain classification using three-dimensional ladar data for ground robot mobility," *J. Field Robot.*, vol. 23, no. 10, pp. 839–862, 2006.

[24] Y. Liu, Q. Dai, and W. Xu, "A point-cloud-based multiview stereo algorithm for free-viewpoint video," *IEEE Trans. Vis. Comput. Graphics*, vol. 16, no. 3, pp. 407–418, May/Jun. 2010.

[25] N. J. Mitra and N. Guyen, "Estimating surface normals in noisy point cloud data," *Int. J. Comput. Geometry Appl.*, vol. 14, nos. 4–5, pp. 261–276, 2004.

[26] G. J. Brostow, J. Shotton, J. Fauqueur, and R. Cipolla, "Segmentation and recognition using structure from motion point clouds," in *Proc. ECCV*, 2008, pp. 44–57.

[27] N. Elmqvist and P. Tsigas, "A taxonomy of 3D occlusion management for visualization," *IEEE Trans. Vis. Comput. Graphics*, vol. 14, no. 5, pp. 1095–1109, Sep./Oct. 2008.

[28] S. Katz, A. Tal, and R. Basri, "Direct visibility of point sets," *ACM Trans. Graph.*, vol. 26, no. 3, 2007, Art. no. 24.

[29] R. Mehra, P. Tripathi, A. Sheffer, and N. J. Mitra, "Visibility noisy point cloud data," *Comput. Graph.*, vol. 34, no. 3, pp. 219–230, 2010.

[30] S. Katz and A. Tal, "Improving the visual comprehension of point sets," in *Proc. IEEE CVPR*, Jun. 2013, pp. 121–128.

[31] S. Katz and A. Tal, "On the visibility of point clouds," in *Proc. IEEE ICCV*, Oct. 2015, pp. 1350–1358.

[32] H. Guan, J. Li, Y. Yu, M. Chapman, and C. Wang, "Automated road information extraction from mobile laser scanning data," *IEEE Trans. Intell. Transp. Syst.*, vol. 16, no. 1, pp. 194–205, Feb. 2015.

Pengdi Huang received the M.Sc. degree in optical engineering from Yunnan Normal University, China, in 2013. He is currently working toward the Ph.D. degree in information and communication engineering with Fujian Key Laboratory of Sensing and Computing for Smart Cities and the Department of Communication Engineering, School of Information Science and Engineering, Xiamen University, China. His research interests include computer vision, 3-D point cloud processing, object detection and extraction, and mobile laser scanning data processing.

Ming Cheng (M'14) received the Ph.D. degree in biomedical engineering from Tsinghua University, China, in 2004.

He is an Associate Professor with Fujian Key Laboratory of Sensing and Computing for Smart Cities and the Xiamen Key Laboratory of Geospatial Sensing and Computing, School of Information Science and Engineering, Xiamen University, Xiamen, China. His research interests include remote sensing image processing, point cloud processing, computer vision, and machine learning.

Dr. Cheng has authored over 30 papers in refereed journals and conference proceedings, including IEEE GEOSCIENCE AND REMOTE SENSING LETTERS, *Neurocomputing*, and IGARSS and ISPRS Proceedings.

Yiping Chen received the Ph.D. degree in information and communication engineering from National University of Defense Technology, China, in 2011. She was a Research Assistant with The Chinese University of Hong Kong from 2007 to 2011. She is currently an Assistant Professor with the National University of Defense Technology and a Post-Doctoral Fellow with the Fujian Key Laboratory of Sensing and Computing for Smart Cities, School of Information Science and Engineering, Xiamen University, China. Her research interests include image processing, mobile laser scanning data analysis, and automated detection of 3-D objects in point clouds.

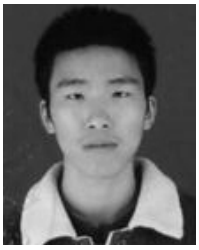

Huan Luo received the B.Sc. degree in computer science from Nanchang University, China, in 2009. He is currently working toward the Ph.D. degree with Fujian Key Laboratory of Sensing and Computing for Smart Cities, School of Information Science and Engineering, Xiamen University, China. His research interests include computer vision, machine learning, and mobile LiDAR point clouds data processing.

Cheng Wang (M'04–SM'16) received the Ph.D. degree in information and communication engineering from National University of Defense Technology, China, in 2002.

He is a Professor with the Fujian Key Laboratory of Sensing and Computing for Smart Cities and an Associate Dean of the School of Information Science and Technology, Xiamen University, China. His research interests include remote sensing image processing, mobile LiDAR data analysis, and multisensor fusion.

Dr. Wang has co-authored about 150 papers published in refereed journals, such as IEEE TRANSACTIONS ON GEOSCIENCE AND REMOTE SENSING, IEEE TRANSACTIONS ON INTELLIGENT TRANSPORTATION SYSTEMS, IEEE GEOSCIENCE AND REMOTE SENSING LETTERS, IEEE JOURNAL OF SELECTED TOPICS IN APPLIED EARTH OBSERVATIONS AND REMOTE SENSING, and *ISPRS Journal of Photogrammetry and Remote Sensing* and conferences, such as IGARSS and ISPRS. He is a Council Member of the Chinese Society of Image and Graphics. He is the Chair of the ISPRS Working Group I/6 on Multisensor Integration and Fusion from 2016 to 2020.

Jonathan Li (M'00–SM'11) received the Ph.D. degree in geomatics engineering from University of Cape Town, South Africa, in 2000.

He is a Professor with Fujian Key Laboratory of Sensing and Computing for Smart Cities, School of Information Science and Engineering, Xiamen University, Xiamen, China. He is also a Professor and the Head of the WatMos Laboratory, Faculty of Environment, University of Waterloo, Waterloo, ON, Canada. His research interests include information extraction from LiDAR point clouds and earth observation images.

Dr. Li has co-authored over 300 publications, over 130 of which were published in refereed journals, including IEEE TRANSACTIONS ON GEOSCIENCE AND REMOTE SENSING, IEEE TRANSACTIONS ON INTELLIGENT TRANSPORTATION SYSTEMS (IEEE-TITS), IEEE GEOSCIENCE AND REMOTE SENSING LETTERS, IEEE JOURNAL OF SELECTED TOPICS IN APPLIED EARTH OBSERVATIONS AND REMOTE SENSING, *ISPRS Journal of Photogrammetry and Remote Sensing*, *International Journal of Reliability and Safety*, *Photogrammetric Engineering & Remote Sensing*, and *Remote Sensing Of Environment*. He is the Chair of the ISPRS Working Group I/2 on LiDAR-, Air- and Spaceborne Optical Sensing from 2016 to 2020, the Chair of the ICA Commission on Sensor-driven Mapping from 2015 to 2019, and an Associate Editor of the IEEE TRANSACTIONS ON INTELLIGENT TRANSPORTATION SYSTEMS and IEEE JOURNAL OF SELECTED TOPICS IN APPLIED EARTH OBSERVATIONS AND REMOTE SENSING.